Constraints on the Decay of 180mTa

I. J. Arnquist, F. T. Avignone III, And S. Barabash, C. J. Barton, K. H. Bhimani, E. Blalock, B. Bos, M. Busch, M. Buuck, In T. S. Caldwell, C. D. Christofferson, P.-H. Chu, M. L. Clark, C. Cuesta, J. J. A. Detwiler, U. Efremenko, A. H. Ejiri, S. R. Elliott, G. K. Giovanetti, J. Goett, M. P. Green, A. Hostiuc, J. Gruszko, G. I. S. Guinn, K. E. Guiseppe, C. R. Haufe, R. Henning, G. D. Hervas Aguilar, E. W. Hoppe, A. Hostiuc, U. Kim, L. Kim, L. K. R. T. Kouzes, T. E. Lannen V., A. Li, G. J. M. López-Castaño, R. Massarczyk, L. J. Meijer, M. Meijer, M. Meijer, L. K. Oli, L. S. Paudel, W. Pettus, A. W. P. Poon, L. C. Radford, A. L. Reine, K. Rielage, A. Rouyer, M. W. Ruof, L. V. Ruof, D. C. Schaper, S. J. Schleich, T. A. Smith-Gandy, L. T. C. Wiseman, U. W. Xu, and C.-H. Yu.

(MAJORANA COLLABORATION)

D. S. M. Alves, ¹² L. Hebenstiel, ^{12,17} and H. Ramani ²⁰ ¹Pacific Northwest National Laboratory, Richland, Washington 99354, USA ²Department of Physics and Astronomy, University of South Carolina, Columbia, South Carolina 29208, USA ³Oak Ridge National Laboratory, Oak Ridge, Tennessee 37830, USA ⁴National Research Center "Kurchatov Institute," Kurchatov Complex of Theoretical and Experimental Physics, Moscow 117218, Russia ⁵Department of Physics, University of South Dakota, Vermillion, South Dakota 57069, USA ⁶Department of Physics and Astronomy, University of North Carolina, Chapel Hill, North Carolina 27514, USA ⁷Triangle Universities Nuclear Laboratory, Durham, North Carolina 27708, USA ⁸Department of Physics, North Carolina State University, Raleigh, North Carolina 27695, USA ⁹Department of Physics, Duke University, Durham, North Carolina 27708, USA ¹⁰Center for Experimental Nuclear Physics and Astrophysics, and Department of Physics, University of Washington, Seattle, Washington 98195, USA 11 South Dakota Mines, Rapid City, South Dakota 57701, USA ¹²Los Alamos National Laboratory, Los Alamos, New Mexico 87545, USA ¹³Centro de Investigaciones Energéticas, Medioambientales y Tecnológicas, CIEMAT 28040, Madrid, Spain ⁴Department of Physics and Astronomy, University of Tennessee, Knoxville, Tennessee 37916, USA ⁵Research Center for Nuclear Physics, Osaka University, Ibaraki, Osaka 567-0047, Japan ¹⁶Physics Department, Williams College, Williamstown, Massachusetts 01267, USA ¹⁷IU Center for Exploration of Energy and Matter, and Department of Physics, Indiana University, Bloomington, Indiana 47405, USA ¹⁸Nuclear Science Division, Lawrence Berkeley National Laboratory, Berkeley, California 94720, USA ¹⁹Joint Institute for Nuclear Research, Dubna 141980, Russia ²⁰Stanford Institute for Theoretical Physics, Stanford University, Stanford, California 94305, USA

(Received 2 June 2023; revised 15 August 2023; accepted 12 September 2023; published 11 October 2023)

 180m Ta is a rare nuclear isomer whose decay has never been observed. Its remarkably long lifetime surpasses the half-lives of all other known β and electron capture decays due to the large K-spin differences and small energy differences between the isomeric and lower-energy states. Detecting its decay presents a significant experimental challenge but could shed light on neutrino-induced nucleosynthesis mechanisms, the nature of dark matter, and K-spin violation. For this study, we repurposed the Majorana Demonstrator, an experimental search for the neutrinoless double-beta decay of 76 Ge using an array of high-purity germanium detectors, to search for the decay of 180m Ta. More than 17 kg, the largest amount of tantalum metal ever used for such a search, was installed within the ultralow-background detector array. In this Letter, we present results from the first year of Ta data taking and provide an updated limit for the 180m Ta half-life on the different decay channels. With new limits up to 1.5×10^{19} yr, we improved existing limits by 1-2 orders of magnitude which are the most sensitive searches for a single β and electron capture decay ever achieved. Over all channels, the decay can be excluded for $T_{1/2} < 0.29 \times 10^{18}$ yr.

DOI: 10.1103/PhysRevLett.131.152501

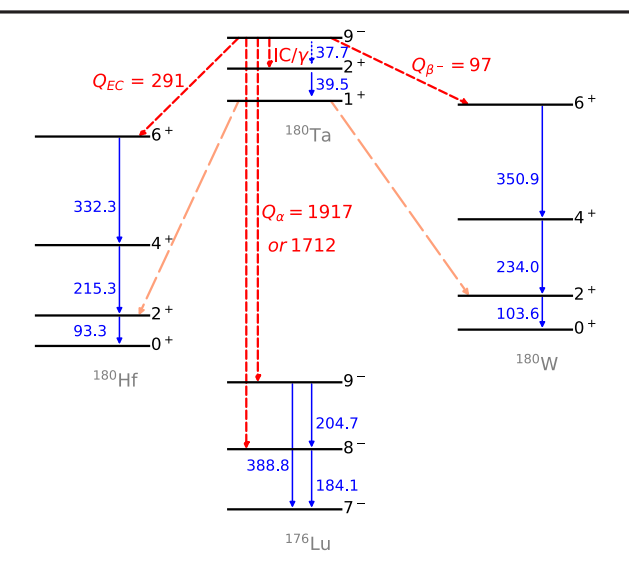


FIG. 1. Level diagram of the decay modes of 180m Ta (red arrows) based on data from Ref. [16]. Certain decay modes can also be observed indirectly when the ground state of 180 Ta is populated that then decays further (pink dashed arrows). The observation of γ rays at characteristic energies can be used to identify the different signatures (blue arrows, blue dashed for the not yet observed 37.7-keV transition). The nomenclature follows Eq. (1), and all energies are given in keV.

The ^{180m}Ta isomer is unique in two interesting ways: It is the only naturally occurring long-lived isomer, and it is the only known isomer that has not been observed to decay, while its ground state has a half-life of only 8.15 h [1]. This remarkable property can be attributed to a combination of two factors: the large difference in the K spin, which stands for the projection of the spin on the symmetry axis, and the small energy differences requiring an *E7* or *M8* transition between the isomeric and lower-lying states [2–4]. The combination of both results in the isomer being trapped in a metastable excited state. Over the past century, numerous attempts were made to measure the decay of ^{180m}Ta [5–11].

As shown in Fig. 1, 180m Ta has several possible decay modes. These include deexcitation to a lower-lying state by γ -ray emission or internal conversion (IC), electron-capture (EC) decay to 180 Hf, to 180 W by β^- decay, and α decay to 176 Lu. As shown in Table I, the IC mode is expected to be the fastest decay, and the γ -ray emission is expected to be the slowest [12,13]. While often neglected, the possibility of an α decay branch is motivated by a positive Q value and the observation of α decays with 10^{18} -yr half-lives in neighboring W isotopes [14]. We follow the common behavior of α decays that similar spin and parity in the daughter are preferred, and, hence, a specific state in 176 Lu is favored; see Fig. 1. The total decay width of the 180m Ta isomer can be expressed as

$$1/T = \Gamma_{\text{total}} = \Gamma_{\text{EC}} + \Gamma_{\beta^{-}} + \Gamma_{\gamma} + \Gamma_{\text{IC}} + \Gamma_{\alpha} + \Gamma_{\text{DM}}. \tag{1}$$

Here, Γ_{EC} and Γ_{β^-} are the decay widths of the isomeric state directly to Hf by EC and β^- decay to W, respectively. The decay width Γ_{γ} and Γ_{IC} are isomeric transitions to lowerlying states of ¹⁸⁰Ta via γ -ray emission or IC, respectively. Γ_{α} is the α decay width, and Γ_{DM} is the decay due to the possible isomeric deexcitation by dark matter (DM) [15]. Each decay mode can be identified by characteristic γ rays; cf. Fig. 1. If no decay is found, the total width has to be bigger than the smallest half-life limit.

Theoretical techniques [13,20] have been proposed for estimating the lifetime of deformed nuclei like ^{180m}Ta. A measurement of the ^{180m}Ta decay rate would test the accuracy of these models, particularly the K-selection rule based on the symmetry of the deformation [13], under the most extreme conditions. In addition, long-lived isomers can be used to constrain DM models by considering the contributions of DM-induced transitions on the decay rate [15]. Finally, the measurement of the ^{180m}Ta lifetime could help explain the observed abundance of ¹⁸⁰Ta and its role within a nucleosynthesis framework [21–24].

Despite being an isotope of interest for almost a century, measuring the decay of the metastable isomer is experimentally challenging. The natural isotopic abundance is very small [23], and obtaining sufficient quantities of the isotope is difficult. Additionally, the expected energies of the decay emissions are low, while the density and atomic number of tantalum metal are high, which makes it challenging to maintain reasonable detection efficiency while increasing the sample mass due to self-shielding. Finally, the decay rate is very slow, making standard radioassay techniques insufficient for detection. To overcome these, a larger amount of material then ever before was installed into the ultralow-background environment of the Majorana Demonstrator. The purpose of Majorana was to demonstrate the feasibility of using enriched high-purity germanium (HPGe) detectors for a ton-scale neutrinoless double-beta decay search in ⁷⁶Ge [25,26]. Located deep underground at the Sanford Underground Laboratory [27], it consisted of two arrays of HPGe detectors in vacuum cryostats within a passive copper, lead, and polyethylene shield as well as an active muon veto. The success of the Demonstrator was enabled by the careful selection and development of ultralow-background components [28], the use of low-noise electronics and data acquisition hardware [29], and excellent energy resolution achieved through a combination of detector design and novel analysis techniques [30,31]. These features also made it an ideal platform for investigating the decay of ¹⁸⁰mTa. Following data taking with the enriched detectors [32] and the removal of the enriched detectors for use in LEGEND-200 [33], the Demonstrator was repurposed to make this measurement in 2022.

To implement tantalum in the existing setup, 99.995% pure Ta metal disks were purchased from Goodfellow Corporation [34]. Each disk is 2 mm thick with a mass

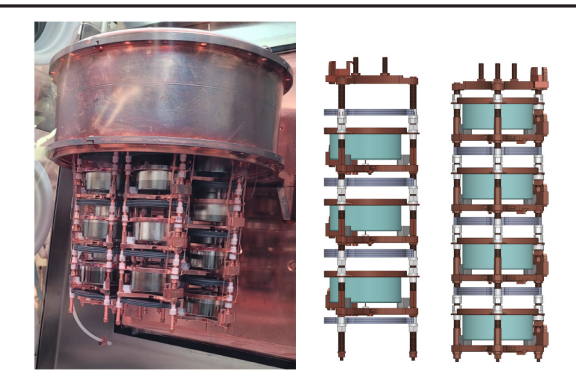


FIG. 2. Left: the detector module during assembly. Right: technical drawing of two of the seven installed strings detector arrangement with three and four HPGe detectors (teal) and the tantalum sample disks (gray).

of approximately 181 g. They were brought underground in January 2022, where they underwent a multistep cleaning process. The disks were scrubbed with Micro-90 to remove oil and manufacturing dirt, then underwent a light chemical etch using 10% nitric acid, and were finally baked under high vacuum. A total of 17.39 kg of Ta disks were installed within the Demonstrator, resulting in a total ^{180m}Ta mass of 2.045 g, assuming a ^{180m}Ta natural abundance of 0.0001176(23) [35], which is a combined analysis of several previous measurements [36–39].

To maximize exposure and detection efficiency while preserving the low-background performance of the Demonstrator, previously screened, ultrahigh-radiopurity components to hold the samples and interleave them with the 23 remaining natural detectors [40]. A Geant4 [41] simulation was used to determine the optimal arrangement while respecting the weight and geometry constraints of the Demonstrator cryostat. It optimizes the thickness of the Ta samples against efficiency for detecting the low-energy γ rays of interest. Figure 2 shows the final configuration. Ta stacks in neighboring strings are offset vertically so that each has a line of sight with at least three detectors.

This Letter presents data collected over 347.8 days between May 2022 and April 2023. Each of the 23 HPGe detectors in the array is read out independently, in a similar fashion to the Majorana Demonstrator experiment. Detector waveforms that exceed approximately 5 keV are digitized with GRETINA digitizers [42,43] and read out using the ORCA (Object-oriented Real-time Control and Acquisition) data acquisition software [44]. Time stamps are synchronized across the data acquisition system, and signals from multiple detectors that occur within a 4 µs window are grouped. Events coincident with muons that trigger the external veto system are tagged for offline removal. Periods of high noise due to liquid-nitrogen fills are also excluded from the analysis. Throughout the data-taking period, a biweekly, 4-h energy calibration was performed with a ²²⁸Th line source [45].

The ^{180m}Ta data analysis was done using the secondary analysis chain of Majorana Demonstrator, a Radware-based software package [46]. Data from ²²⁸Th calibration data was used to set the energy scale for each subsequent twoweek period. The energy calibration procedure uses many of the tools developed for the Demonstrator, including pole-zero and charge-trapping corrections [31]. To estimate the quality of the energy calibration, the γ rays from natural backgrounds (which are not used for calibration), including ¹⁸²Ta, are fit with one or more Gaussian functions plus a linear background. For the lowest energies, an additional exponential background component is added to reproduce the rise of the spectrum toward lower energies. For each energy, the width of the Gaussian agrees well with the resolution achieved during the neutrinoless double-beta decay search [31] and results in a FWHM of 0.4 keV at 100 keV. Three of the 23 detectors showed gain drifts following a power outage that occurred midway through data taking, which negatively affected their energy resolution, and these detectors were not used in this analysis.

Following energy calibration, the data are checked for dropout periods by measuring the event rate. If no events occur within a detector over a 4-h window, that entire time period, for all detectors, is excluded from the analysis. Beside calibrations, one-day shutdowns due to power outages impacted the life time. The array was live for 98.2% of the data-taking period as a result of these cuts.

A 10-keV analysis threshold is applied to all datasets, and the data are blinded by removing events that fall within ± 2 keV of signature γ rays. The possible decay modes and the subsequent γ rays are shown in Fig. 1: EC to ¹⁸⁰Hf γ rays are 93.3, 215.3, and 332.2 keV; β^- decay to ¹⁸⁰W γ rays are 103.6, 234.0, and 350.9 keV; and internal γ rays are 37.7 and 39.5 keV [16]. For the IC, only the 39.5 keV transition can be observed. An additional signature of the γ and IC branches is the observation of a 93.3- or a 103.6-keV γ ray from the deexcitation of Hf or W, although the branching ratios to the first excited states of these nuclei is small (25% for Hf and 4% for W).

The total event rate of a few hertz observed in the detector array is dominated by signals originating from the Ta samples; see Fig. 3. There is a constant event rate due to long-lived natural radioactivity in the disks and apparatus. From the Demonstrator data, we can estimate that in the current configuration only about 10% of the observed constant background comes from the latter; hence, the sample disks contain around 0.5(1) mBq/kg_{Ta} ²³⁸U and 0.10(2) mBq/kg_{Ta} ²³²Th. The decrease of the background rate is due to ¹⁸²Ta and ¹⁷⁵Hf, which are the remnants of cosmogenic activation of the Ta samples above ground, with half-lives of 114 and 70.3 days, respectively. Previous studies stored their Ta samples underground for several years before beginning measurements to eliminate these backgrounds [47].

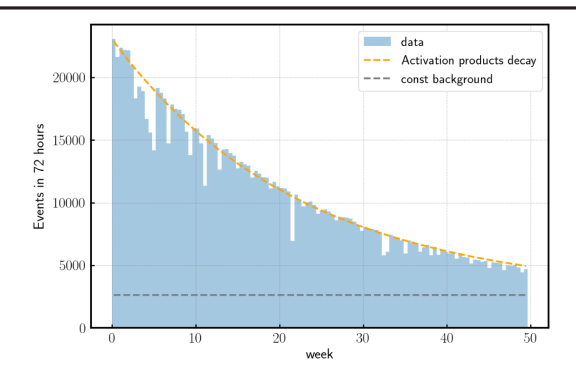


FIG. 3. Count rate in real time for the region between 100 and 500 keV, where the ^{180m}Ta signatures are expected. The count rate, not lifetime corrected, is due primarily to radioactivity in the Ta samples: ¹⁸²Ta decay, the decay of other short-lived cosmogenic isotopes, and a constant rate from the U/Th decay chains.

A crucial component of the half-life calculation is the efficiency for detecting the signature γ rays emitted during the 180m Ta decay under exclusion of possible summing of signals in the cascades. To determine this, a combination of experimental data and Monte Carlo simulation is used. First, a Geant4 simulation was performed in which individual γ rays were emitted from uniformly distributed points within the Ta disks. The starting energy of the γ rays was varied from 10 keV to 3 MeV in increments of 10 keV, and the efficiency of detecting these γ rays in one of the detectors was calculated at each energy. The resulting interpolated efficiency curve is shown in Fig. 4. The simulation assumes the cosmogenic activity is uniform between all of the Ta disks, which is consistent with the observed count rates in each detector.

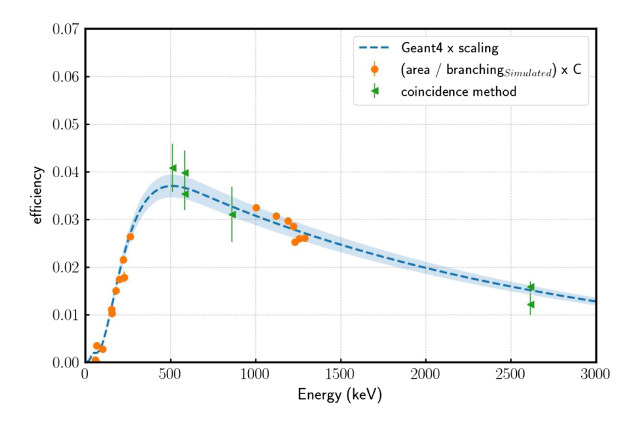


FIG. 4. Simulated detection efficiency averaged per detector (blue dashed line) compared to the intensities of γ rays from ¹⁸²Ta decays with branching ratio greater than 1% (orange points). Since the absolute ¹⁸²Ta activity is not known, the points are multiplied with an arbitrary constant C to compare the distribution to the curve shape. The green points show efficiencies determined by the ²⁰⁸Tl coincidence method. The simulation is normalized to these points [scaling factor 0.95(6)], whereas the band represents the uncertainty due to scaling.

The shape of the simulated efficiency curve is validated by a comparison with the observed intensities of the γ rays from ¹⁸²Ta decay, after correcting the signal intensities for the known branching ratios (e.g., [48]). The absolute efficiency, or a possible scaling of the predicted curve, is determined using the coincidence method [49,50]. In this method, one compares the individual intensity of γ rays in a cascade with the rate of multidetector events to obtain the absolute efficiency of an individual detector. The ²⁰⁸Tl decay at the end of the natural ²³²Th chain provides cascades that can be used for this analysis. Because of the low rate of ²⁰⁸Tl decays in the Ta disks, this method suffers from low statistics, especially for high multiplicity events, and the uncertainty on the derived efficiencies is large. The Geant4-derived efficiency is normalized to these points using a least-squares fit that results in a scaling of 0.95(6), and the efficiency values from this scaled curve are used in the following analysis.

The ^{180m}Ta half-life can be calculated from the following formula:

$$T_{1/2} = \ln 2 \frac{\epsilon_k b}{S_k} N_{\text{Ta}} T_{\text{live}}, \tag{2}$$

where S_k represents the counts in the kth decay channel, ε_k is the detection efficiency at the energy E for a specific decay mode (shown by the curve in Fig. 4), b is a factor for taking into account the branching ratio as well as the internal conversion probability, and $N_{\rm Ta}$ is the number of 180m Ta atoms, $6.84(17) \times 10^{21}$. The live time of the data-taking period, $T_{\rm live}$, is 341.5 days.

A likelihood fit is used to extract the ^{180m}Ta decay signal strengths from the data. Spectral fits were performed in the region of interest (ROI) surrounding each of the characteristic y-ray energies. The fits include a Gaussian peak shape for the signal, a linear background, and additional Gaussians at the energies of any known background lines in the region of interest; see, e.g., Fig. 5. The literature values for the energy of the γ rays and the expected energy resolution are used as initial values in the fit. The energy is allowed to float within ± 0.5 keV, and the resolution is allowed to float within $\pm 10\%$ from the expected value. The background rate in each detector is fit to be about 0.7 and 0.5 cts/(keV day) averaged over the data-taking period in the 100- and 300-keV region, respectively. This rate is comparable with previous experiments [10]. The fit of the 93.3-keV and the 350.9-keV ^{180m}Ta signals are impacted by nearby background. The excellent energy resolution of the Demonstrator allows a simultaneous fit of multiple contributions from signal and backgrounds at known energies. Hence, all regions can be used, but some will have larger uncertainties. Within all of the signal ROI, the best-fit signal strength is within 2σ of a null result. To calculate S_k , the best-fit peak area plus 1.65 σ (90% C.L.) is used to calculate a limit on the decay rate.

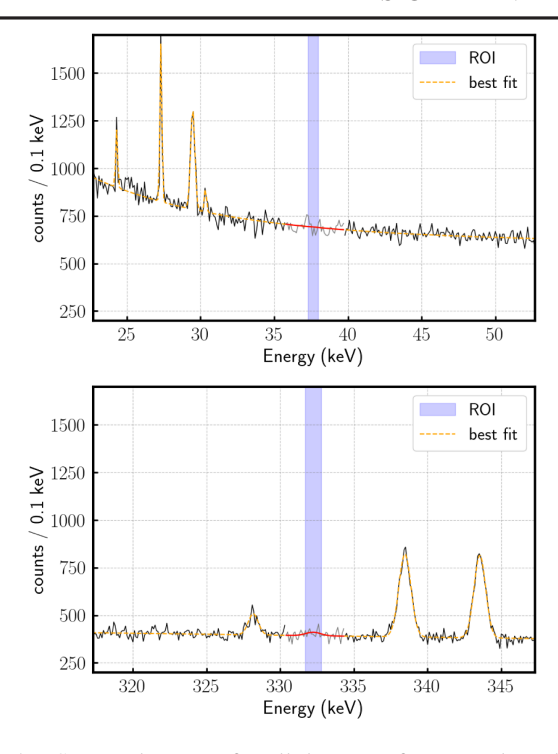


FIG. 5. Summed spectra for all detectors for two selected ROI for the 37.7-keV (top) and the 332.3-keV (bottom) γ rays, respectively. The yellow line shows the best fit of the background peaks and flat background. The red curve shows the best fit of the signal peak.

In contrast to previous studies, the large number of detectors in close geometry combined with low-background rate means a multiplicity analysis can be done that looks for the coincident γ rays expected from some of the 180m Ta decay channels. This analysis is competitive with fitting the single-detector spectra, because the reduction in

signal detection efficiency (0.001–0.01) is counterbalanced by the improved background suppression ($\sim 10^{-3}$ cts/ (keV keV day) so that the ϵ_k/S_k factor is similar to, or higher than, the simple spectral search. A two-dimensional histogram is made for events that contain two coincident energy deposits within the considered signal regions, and a two-dimensional likelihood fit is done assuming the same mean energy and peak resolution as in the one-dimensional fit. The efficiency ϵ from Eq. (2) now consists of the simulated detection efficiency for a two-detector event with the corresponding energies from within the cascade; cf. Fig. 1. In this simulation, two γ rays are started with an angular correlation factor based on multipole momentum and spin of the emitting states [51]. The results from the spectral and two-dimensional fits are shown in Table I. These results improve upon the best existing limits for each decay channel and combine for a total half-life limit of $T_{1/2} > 0.29 \times 10^{18}$ yr. In previous measurements [9,10,52], the total half-life is calculated without considering the isomeric transitions. Reference [52] does search for the isomeric transitions but does not include them in the total half-life calculation. The most recent work [11] includes them; hence, the Majorana Demonstrator result represents an improvement of 2 orders of magnitude. For the direct decays of the isomeric state, the improvement in efficiency and reduction in background rate due to the coincidence method results in an improvement of about one order of magnitude. These improvements are of great interest to the predictions on the basis of the K-selection rules [13].

The nonobservation of the transition to the ground state decays (Γ_{γ} and Γ_{IC}) constrains the phase space of certain classes of DM models that evade traditional underground detection methods [15,47]; cf. Fig. 6. Strongly interacting

TABLE I. Measured decay half-life limits. Results are given at a 90% C.L. using the one-dimensional spectral fits (SF), a multiplicity-two analysis (2D) where applicable, and the strongest limit for the decay channel. The nomenclature introduced in Eq. (1) is used to describe each decay channel. For the 39.5-keV transition (*), the internal conversion factor is calculated using Ref. [17].

Method	EC		β^-		γ		IC		α	
	Energy (keV)	$T_{1/2}$ (10 ¹⁸ yr)	Energy (keV)	$T_{1/2}$ (10 ¹⁸ yr)	Energy (keV)	$T_{1/2}$ (10 ¹⁸ yr)	Energy (keV)	$T_{1/2}$ (10 ¹⁸ yr)	Energy (keV)	$T_{1/2}$ (10 ¹⁸ yr)
SF	93.3	1.23(30)	103.6	1.54(17)	37.7	0.63(8)			184.1	4.80(42)
	215.3	5.69(55)	234.0	5.76(75)	39.5	$0.06(1)^*$	39.5	$0.06(1)^*$	204.7	5.58(54)
	332.2	10.0(13)	350.9	9.31(114)	93.3	0.29(4)	93.3	0.29(4)	388.8	10.2(12)
					103.6	0.07(2)	103.6	0.07(2)		
2D	93.3 + 215.3	1.88(35)	103.6 + 234.0	2.65(49)					184.1 + 204.7	11.3(22)
	93.3 + 332.2	3.18(56)	103.6 + 350.9	4.18(78)						
	215.3 + 332.2	13.3(22)	234.0 + 350.9	15.4(27)		• • •				
Best: this work		13.3(22)		15.4(27)		0.63(8)		0.29(4)		11.3(22)
Previous works		1.6 [11]		1.1 [11]		0.0045 [11]		0.0045 [11]		
Expected $T_{1/2}$ [12,13,18,19]		10^{20} yr		10^{23} yr		10^{31} yr		10^{18-19} yr		10 ²⁸ yr

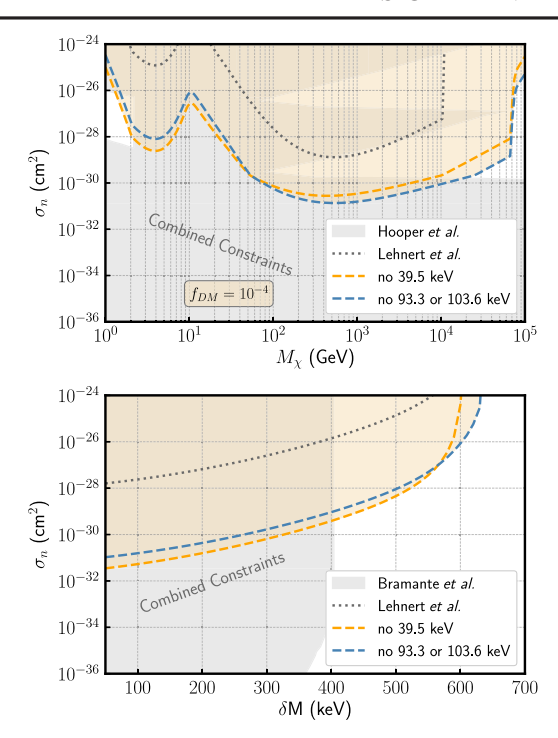


FIG. 6. Top: 90% C.L. exclusion limits on the per-nucleon cross section for strongly interacting DM assuming a fractional relic density of $f_{\rm DM}=10^{-4}$. The limit based on the non-observation of the 93.3-keV line (blue dashed) is sensitive to DM-induced deexcitations to the ¹⁸⁰Ta first excited (2⁺) and ground (1⁺) states. This can be compared to limits from Ref. [47] (gray dashed line), which is based on the 103.5-keV signature. The limit derived from the nonobservation of the 39.5-keV line (dashed orange) is sensitive only to deexcitations to the first excited state. Both cover phase space not covered by other experimental approaches [53]. Bottom: 90% C.L. exclusion limits on the per-nucleon cross section for inelastic DM with mass splitting δM . Color coding is identical to the top plot (the gray shaded region is based on Ref. [54]).

DM, which thermalizes as it passes through Earth, rendering it undetectable via nuclear scattering, would mediate exothermic transitions from the ¹⁸⁰mTa state and measurably increase the decay rate of the isomer. Similarly, in inelastic DM models, ground state DM interacts only inelastically with standard model particles and upscatters to an excited state by downscattering ¹⁸⁰mTa, increasing the measured ¹⁸⁰mTa decay rate.

In summary, we set improved limits on the decay of 180m Ta while deriving stronger constraints on strongly interacting and inelastic dark matter. Data taking with the Demonstrator array will continue into 2024, and, as the background rate decreases further to about a quarter of the current average due to the decay of cosmogenics within the Ta samples, sensitivity will continue to improve. Besides dedicated $\beta\beta$ searches and some α decays, the results presented are the most sensitive search for radioactive decays ever achieved.

We gratefully acknowledge that the research presented in this report was supported by the Laboratory Directed Research and Development program of Los Alamos National Laboratory under Project No. 20220092ER, which enabled the ¹⁸⁰rTa rare decay search. This material is based upon work supported by the U.S. Department of Energy, Office of Science, Office of Nuclear Physics under Contracts or Grants No. DE-AC02-05CH11231, No. DE-AC05-00OR22725, No. DE-AC05-76RL0130, No. DE-FG02-97ER41020, No. DE-FG02-97ER41033, No. DE-FG02-97ER41041, No. DE-SC0012612, No. DE-SC0014445, No. DE-SC0018060, No. DE-SC0022339, and No. LANLEM77/LANLEM78. We acknowledge support from the Particle Astrophysics Program and Nuclear Physics Program of the National Science Foundation through Grants No. MRI-0923142, No. PHY-1003399, No. PHY-1102292, No. PHY-1206314, No. PHY-1614611, No. PHY-1812409, No. PHY-1812356, No. PHY-2111140, and No. PHY-2209530. We gratefully acknowledge the support of the Laboratory Directed Research and Development (LDRD) program at Lawrence Berkeley National Laboratory for this work. We gratefully acknowledge the support of the U.S. Department of Energy through the Los Alamos National Laboratory LDRD Program, the Oak Ridge National Laboratory LDRD Program, and the Pacific Northwest National Laboratory LDRD Program for this work. We gratefully acknowledge the support of the South Dakota Board of Regents Competitive Research Grant. We acknowledge the support of the Natural Sciences and Engineering Research Council of Canada, funding Reference No. SAPIN-2017-00023, and from the Canada Foundation for Innovation John R. Evans Leaders Fund. We acknowledge support from the 2020/ 2021 L'Oréal-UNESCO for Women in Science Program. This research used resources provided by the Oak Ridge Leadership Computing Facility at Oak Ridge National Laboratory and by the National Energy Research Scientific Computing Center, a U.S. Department of Energy Office of Science User Facility. We thank our hosts and colleagues at the Sanford Underground Research Facility for their support.

^{*}Present address: Lawrence Livermore National Laboratory, Livermore, California 94550, USA.

^{*}Corresponding author: massarczyk@lanl.gov

[‡]Present address: Argonne National Laboratory, Lemont, Illinois 60439, USA.

^[1] C. Gallagher, M. Jørgensen, and O. Skilbreid, A measurement of β — and ec branching ratios in the decay of 8.15-h ta180 and a search for the β — decay of hf180m, Nucl. Phys. **33**, 285 (1962).

^[2] P. Walker and G. Dracoulis, Energy traps in atomic nuclei, Nature (London) **399**, 35 (1999).

- [3] P. M. Walker, G. D. Dracoulis, and J. J. Carroll, Interpretation of the excitation and decay of 180 Ta m through a $k^{\pi} = 5^+$ band, Phys. Rev. C **64**, 061302(R) (2001).
- [4] M. L. Bissell *et al.*, Model independent determination of the spin of the ¹⁸⁰Ta naturally occurring isomer, Phys. Rev. C 74, 047301 (2006).
- [5] E. R. Bauminger and S. G. Cohen, Natural radioactivity of V⁵⁰ and Ta¹⁸⁰, Phys. Rev. 110, 953 (1958).
- [6] T. B. Ryves, The decay scheme of ^{180m}Ta, J. Phys. G **6**, 763 (1980).
- [7] J. B. Cumming and D. E. Alburger, Search for the decay of ¹⁸⁰Ta^m, Phys. Rev. C 31, 1494 (1985).
- [8] M. Wakasugi, W. G. Jin, T. T. Inamura, T. Murayama, T. Wakui, H. Katsuragawa, T. Ariga, T. Ishizuka, and I. Sugai, Precision measurement of the hyperfine structure and nuclear moments of ¹⁸⁰mTa by laser-rf double resonance, Phys. Rev. A 50, 4639 (1994).
- [9] M. Hult, J. Gasparro, G. Marissens, P. Lindahl, U. Watjen, P. N. Johnston, C. Wagemans, and M. Kohler, Underground search for the decay of ¹⁸⁰Ta^m, Phys. Rev. C 74, 054311 (2006).
- [10] B. Lehnert, M. Hult, G. Lutter, and K. Zuber, Search for the decay of nature's rarest isotope ^{180m}Ta, Phys. Rev. C 95, 044306 (2017).
- [11] R. Cerroni *et al.*, Deep-underground search for the decay of 180m-ta with an ultra-low-background HPGe detector, arXiv:2305.17238.
- [12] N. Auerbach and V. Zelevinsky, The curious case of tantalum 180, AIP Conf. Proc. 1912, 020002 (2017).
- [13] H. Ejiri and T. Shima, K-hindered beta and gamma transition rates in deformed nuclei and the halflife of ¹⁸⁰Ta^m, J. Phys. G **44**, 065101 (2017).
- [14] C. Cozzini *et al.*, Detection of the natural alpha decay of tungsten, Phys. Rev. C **70**, 064606 (2004).
- [15] M. Pospelov, S. Rajendran, and H. Ramani, Metastable nuclear isomers as dark matter accelerators, Phys. Rev. D 101, 055001 (2020).
- [16] E. McCutchan, Nuclear data sheets for a = 180, Nucl. Data Sheets 126, 151 (2015).
- [17] T. Kibédi, T. Burrows, M. Trzhaskovskaya, P. Davidson, and C. Nestor, Evaluation of theoretical conversion coefficients using BrIcc, Nucl. Instrum. Methods Phys. Res., Sect. A 589, 202 (2008).
- [18] G. Royer, Analytic expressions for alpha-decay half-lives and potential barriers, Nucl. Phys. A848, 279 (2010).
- [19] T. Fényes and Z. Bődy, Expected α-decay data of the rare earth nuclides on the basis of different systematics, Acta Physica Academiae Scientiarum Hungaricae **16**, 299 (1964).
- [20] H. Ejiri, J. Suhonen, and K. Zuber, Neutrino–nuclear responses for astro-neutrinos, single beta decays and double beta decays, Phys. Rep. 797, 1 (2019).
- [21] P. Mohr, F. Kappeler, and R. Gallino, Survival of nature's rarest isotope ¹⁸⁰Ta under stellar conditions, Phys. Rev. C **75**, 012802(R) (2007).
- [22] T. Hayakawa, P. Mohr, T. Kajino, S. Chiba, and G. J. Mathews, Reanalysis of the (j = 5) state at 592 kev in 180 Ta and its role in the ν -process nucleosynthesis of 180 Ta in supernovae, Phys. Rev. C **82**, 058801 (2010).

- [23] G. Baccolo, Tantalizing tantalum, Nat. Chem. 7, 854 (2015).
- [24] K. Malatji *et al.*, Re-estimation of ¹⁸⁰Ta nucleosynthesis in light of newly constrained reaction rates, Phys. Lett. B **791**, 403 (2019).
- [25] N. Abgrall *et al.* (Majorana Collaboration), The Majorana Demonstrator neutrinoless double-beta decay experiment, Adv. High Energy Phys. **2014**, 365432 (2014).
- [26] S. I. Alvis *et al.* (Majorana Collaboration), A search for neutrinoless double-beta decay in ⁷⁶Ge with 26 kg-yr of exposure from the Majorana demonstrator, Phys. Rev. C **100**, 025501 (2019).
- [27] J. Heise, The Sanford underground research facility at homestake, J. Phys. Conf. Ser. **606**, 012015 (2015).
- [28] N. Abgrall *et al.*, The Majorana Demonstrator radioassay program, Nucl. Instrum. Methods Phys. Res., Sect. A 828, 22 (2016).
- [29] N. Abgrall *et al.* (Majorana Collaboration), The Majorana Demonstrator readout electronics system, J. Instrum. 17, T05003 (2022).
- [30] N. Abgrall *et al.*, Adc nonlinearity correction for the Majorana Demonstrator, IEEE Trans. Nucl. Sci. 68, 359 (2021).
- [31] I. J. Arnquist *et al.* (Majorana Collaboration), Charge trapping correction and energy performance of the Majorana Demonstrator, Phys. Rev. C **107**, 045503 (2023).
- [32] I. J. Arnquist *et al.* (Majorana Collaboration), Final Result of the Majorana Demonstrator's Search for Neutrinoless Double-β Decay in Ge76, Phys. Rev. Lett. **130**, 062501 (2023).
- [33] N. Abgrall *et al.*, The large enriched germanium experiment for neutrinoless double beta decay (LEGEND), AIP Conf. Proc. **1894**, 020027 (2017).
- [34] Goodfellow Corporation, https://www.goodfellow.com/us/en-us.
- [35] Pubchem element summary for atomic number 73, tantalum (2023), https://pubchem.ncbi.nlm.nih.gov/element/Tantalum/#section=Historical-Isotopic-Abundances.
- [36] N. Holden, Atomic weights of the elements 1979, Pure Appl. Chem. 52, 2349 (1980).
- [37] M. Berglund and M. E. Wieser, Isotopic compositions of the elements 2009 (IUPAC technical report), Pure Appl. Chem. 83, 397 (2011).
- [38] M. Pfeifer, N. S. Lloyd, S. T. M. Peters, F. Wombacher, B.-M. Elfers, T. Schulz, and C. Münker, Tantalum isotope ratio measurements and isotope abundances determined by mc-icp-ms using amplifiers equipped with 1010, 1012 and 1013 ohm resistors, J. Anal. At. Spectrom. 32, 130 (2017).
- [39] J. R. de Laeter and N. Bukilic, Isotope abundance of ¹⁸⁰Ta^m and p-process nucleosynthesis, Phys. Rev. C **72**, 025801 (2005).
- [40] Canberra Industries Inc. (now Mirion Technologies), https://www.mirion.com/products/bege-broad-energy-germanium-detectors.
- [41] S. Agostinelli *et al.* (Geant4 Collaboration), Geant4—A simulation toolkit, Nucl. Instrum. Methods Phys. Res., Sect. A **506**, 250 (2003).
- [42] D. Doering, J. Joseph, H. Yaver, and S. Zimmermann, GRETINA digitizer specification, Technical Report No. GRT-3-060815-0, Gamma Ray Energy Tracking

- In-Beam Nuclear Array, Nuclear Science Division, Lawrence Berkeley National Laboratory, Berkeley, 2008.
- [43] J. Anderson, R. Brito, D. Doering, T. Hayden, B. Holmes, J. Joseph, H. Yaver, and S. Zimmermann, Data acquisition and trigger system of the gamma ray energy tracking inbeam nuclear array (GRETINA), IEEE Trans. Nucl. Sci. 56, 258 (2009).
- [44] M. A. Howe, G. A. Cox, P. J. Harvey, F. McGirt, K. Rielage, J. F. Wilkerson, and J. M. Wouters, Sudbury neutrino observatory neutral current detector acquisition software overview, IEEE Trans. Nucl. Sci. 51, 878 (2004).
- [45] N. Abgrall *et al.*, The Majorana Demonstrator calibration system, Nucl. Instrum. Methods Phys. Res., Sect. A 872, 16 (2017).
- [46] RadWare/ORNL analysis codes for Majorana Demonstrator (MJD) data analysis and HPGe detector characterization., https://github.com/radforddc/rw0nbb.
- [47] B. Lehnert, H. Ramani, M. Hult, G. Lutter, M. Pospelov, S. Rajendran, and K. Zuber, Search for Dark Matter Induced Deexcitation of ¹⁸⁰Ta^m, Phys. Rev. Lett. **124**, 181802 (2020).

- [48] B. Singh, Nuclear data sheets for a = 182, Nucl. Data Sheets **130**, 21 (2015).
- [49] V. V. Golovko, Simplified efficiency calibration methods for semiconductor detectors used in criticality dosimetry, Appl. Radiat. Isot. 187, 110335 (2022).
- [50] S. Hlavac, Coincidence method for semiconductor detector calibration, Technical Report No. iNDC(NDS)-403, International Atomic Energy Agency (IAEA), 1999.
- [51] A. Bohr and B. Mottelson, *Nuclear Structure*, Vol. 1 (W. A. Benjamin, New York/Amsterdam, 1969).
- [52] M. Hult, J. E. Wieslander, G. Marissens, J. Gasparro, U. Watjen, and M. Misiaszek, Search for the radioactivity of ^{180m}Ta using an underground HPGe sandwich spectrometer, Appl. Radiat. Isot. 67, 918 (2009).
- [53] D. Hooper and S. D. McDermott, Robust constraints and novel gamma-ray signatures of dark matter that interacts strongly with nucleons, Phys. Rev. D 97, 115006 (2018).
- [54] J. Bramante, P. J. Fox, G. D. Kribs, and A. Martin, Inelastic frontier: Discovering dark matter at high recoil energy, Phys. Rev. D 94, 115026 (2016).